COBEM 2021 26th International Congress of Mechanical Engineering
November 22-26, 2021, Virtual Congress, Brazil

COB-2021-0087
3D PRINTED HEXAPOD ROBOT ACTUATED BY SHAPE MEMORY ALLOY SPRINGS: DESIGN AND PERFORMANCE ANALYSIS

Edilberto Alves de Abrantes Júnior
Augusto Figueiredo Emiliavaca
Universidade Federal de Campina Grande, R. Aprígio Veloso, 882 - Universitário, Campina Grande - PB, 58429-140.
edilberto.a.jr@gmail.com
augustoemiliavaca@hotmail.com

Carlos José de Araújo
Universidade Federal de Campina Grande, R. Aprígio Veloso, 882 - Universitário, Campina Grande - PB, 58429-140.
carlos.araujo@ufcg.edu.br

Raimundo Nonato Calazans Duarte
Universidade Federal de Campina Grande, R. Aprígio Veloso, 882 - Universitário, Campina Grande - PB, 58429-140.
raimundo.duarte@ufcg.edu.br

Abstract. *The increasing development of robots in the most diverse areas has encouraged the search for different ways to conceive the design of these sophisticated structures. In this scenario, the present work will show the design, fabrication and tests of a robot prototype made by 3D printing using the polymer Acrylonitrile Butadiene Styrene (ABS) which is actuated by resistive heating of NiTi shape memory alloy (SMA) micro springs. An experimental analysis was performed by using the concept of compliant mechanisms to get movement in the prototype. The prototype showed a satisfactory performance, although it needs some future improvements.*

Keywords: *Hexapod robot, shape memory alloy, 3D printing, compliant mechanisms, ABS.*

1. INTRODUCTION

The use of additive manufacturing (3D printing) in the industry has been increasing due to its advantages of minimizing material waste, rapid prototyping, flexibility, high productivity and low costs, in some cases. One of the areas that has been benefiting from this technology is robotics, since there are significant applications such as 3D printed robot parts and building prototypes to test the control systems.

Among the types of actuators used in robotic systems, there is one based in smart materials that has been studied in the last few years: the shape memory alloy (SMA) actuators. The SMAs can present two different phases: martensite (twinned or detwinned), which is the low-temperature phase, and austenite, which is the high-temperature phase. These phases are at the origin of two different behaviors: the shape memory effect (SME), which occurs when the SMA, initially at the martensitic phase, undergoes plastic deformation and then, after heating and reaching the austenitic phase, it recovers the deformation and returns to the martensitic phase after cooling, with the possibility of recovering about 8% deformation (Srinivasan and McFarland, 2001); and the superelastic effect (SE), which occurs when the SMA, initially at the austenitic phase, undergoes mechanical load with large elastic deformation, induced by the transformation of austenitic into martensitic phase, and then, after unloading, it recovers the deformation.

The most common SMA actuators used are wires and springs, and the actuating mechanism consists in using both SME and SE effects. Several authors have proposed some designs for systems actuated by SMA, such as: Reynaerts and Van Brussel (1992) proposed a nickel-titanium (NiTi) actuator for robot hands; Emiliavaca (2016) designed a morphing wing actuated by NiTi micro springs; and Hora (2016) designed a hexapod robot actuated by NiTi micro springs.

To benefit from SMAs as actuators, it is necessary to combine design solutions and proper control techniques. Doroftei and Stirbu (2014), for example, proposed a hexapod robot model focusing on design solutions for the legs, inspired by the biological mechanisms of animals. The legs were modeled to mimic the action of biological muscles and tendons, which resulted in a tree structure leg design composed by two main mechanisms, each one having a spring simulating a tendon and a NiTi wire actuator simulating a muscle.

Motzki (2020) presented both design and control concepts in order to increase the energy efficiency of SMA actuated systems by developing a bistable mechanism consisted of two SMA wires acting antagonistically, switching between two energy-free actuator positions, and a control concept using high-voltage activation pulses, which led to low energy consumption, avoiding high losses to the environment through heat transfer, resulting in energy savings of 60 - 80% when compared to conventional control.

Another subject that has been studied recently and has wide applications in a large number of areas, including robotics, is the compliant mechanisms field. These flexible mechanisms not only transform and transfer energy, but also have the characteristic of having almost zero pin joints, with the advantages of reducing the number of parts from the mechanism, thus reducing the assembly time (some of them can be constructed in one single piece) and costs. Howell (2001) presents several methods for modeling and design different types of compliant mechanisms. Song et al. (2010) developed a voice-coil actuator with a compliant mechanism for Optical Image Stabilization (OIS) in mobile phone cameras, with the purpose of adjusting the camera to compensate the motion from the user. The application of a compliant mechanism in this case made it possible to use an open-loop control due to the frictionless characteristic of the compliant mechanism, which eliminated the need for a position sensor that is required when using prismatic joints, because of the friction that is hard to be defined.

Since compliant mechanisms and SMA actuators share similar characteristics, such as being lightweight, noiseless, frictionless and presenting smooth motion when activated (which can make them a better choice than electromagnetic motors and rigid members to mimic biological mechanisms), it can be advantageous to combine both as it is shown by the finger model designed by Lan and Yang (2009). This finger consists of compliant phalanges actuated by SMA wires emulating muscles. Another point that makes compliant mechanisms and SMA actuators fit well together is the fact that SMA actuators need a restoring force to bring the system back to its initial position when the actuation stops, and the compliant mechanism can work as a bias spring restoring the position when the SMA actuator is no longer being activated. It is how the finger proposed by Lan and Yang (2009) works, with each compliant phalange acting both as an actuated mechanism and a bias spring.

In this sense, the main objective of this work is to design and testing a 3D printed hexapod robot applying the concept of compliant mechanism and using SMA micro springs as electrical actuators. Preliminary tests showed acceptable performance in terms of movement speed, but also revealed the need for improvements from this first prototype.

2. MATERIALS AND METHODS

The robot structure was designed based on the SMArt Robot developed by Hora (2016), as shown in Figure 1. However, in this work the concept of compliant mechanisms (Howell, 2001) was applied to design the novel robot as a single part composed of a body and legs, to be printed in plastic. The electrical actuation of the legs was performed using the same NiTi SMA micro spring actuators employed by Emiliavaca (2016).

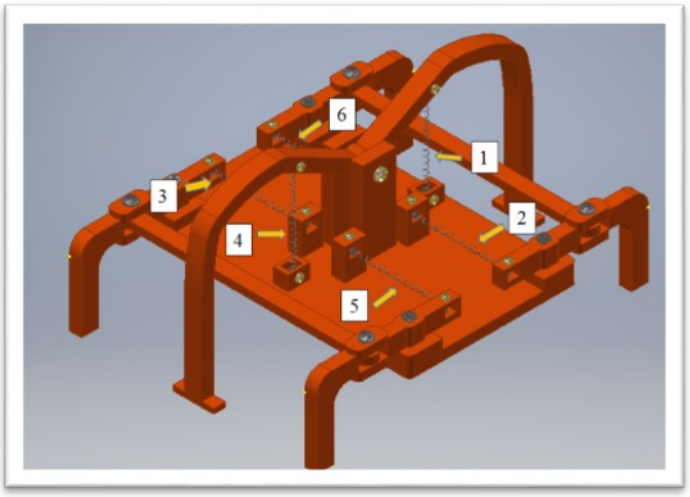

Figure 1. Fully assembled SMArt Robot prototype for testing. The numbers indicate the NiTi SMA micro spring actuators. Hora (2016).

2.1 Materials used for the robot construction

The robot structure was manufactured using acrylonitrile butadiene styrene (ABS), by 3D printing using a MakerBot Replicator 2X Experimental 3D Printer. NiTi micro springs (54.5 – 57.0% Ni), with body length of 7.5 mm and outside diameter of 1.27 mm, were used as actuators. The springs were actuated by resistive heating controlled by a Multifunction I/O device, from National Instruments, with a LabVIEW routine. The electric current was provided by an Agilent power supply.

2.2 Tests and data used for the robot design

To determine the optimal electric current to be used, it was made a set of tests where a NiTi spring was deformed and heated with different currents. Temperature and time were recorded.

The estimated force produced by the NiTi springs was determined by using the data from Emiliavaca (2016).

2.3 Pseudo-rigid-body model

The robot legs were designed using the pseudo-rigid-body model described by Howell (2001), which simplifies the modeling for small-length flexural pivots and considers it as two rigid links joined at a pin point, which is called characteristic pivot and is located at the center of the flexural pivot. The small beam's behavior is modeled as a torsional spring, located at the characteristic pivot, and this model can give accurate results, even for large deflections. This model is illustrated in Figure 2.

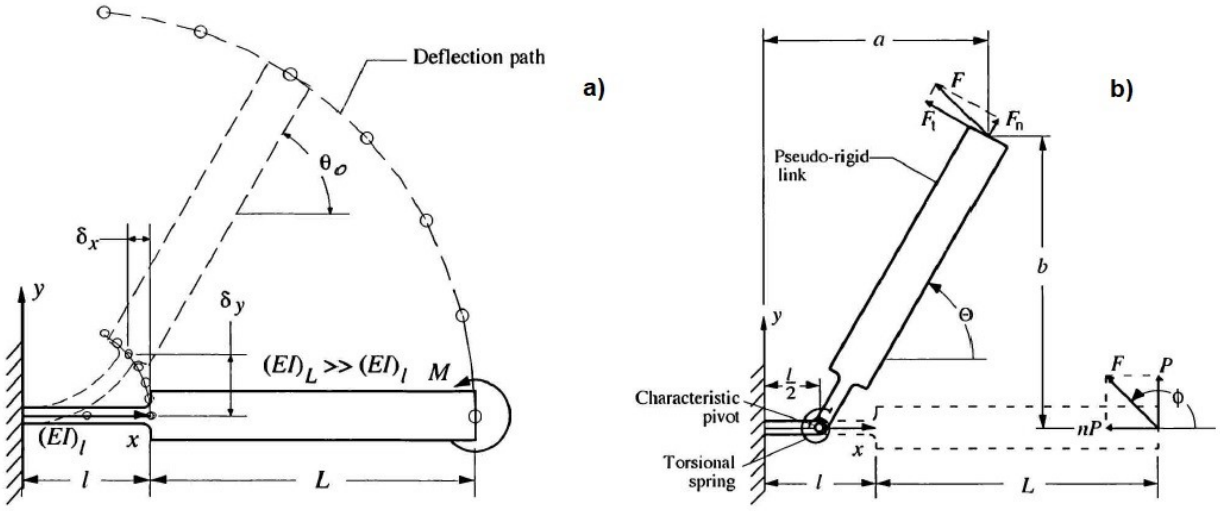

Figure 2. Small-length flexural pivot (a) and the pseudo-rigid-body model with a force at the free end (b). Howell (2001).

The equations for the parameters defined in the model of Figure 2 (b) are the following:

$$a = \frac{l}{2} + \left(L + \frac{l}{2}\right) cos\Theta \tag{1}$$

$$b = \left(L + \frac{l}{2}\right) sen\Theta \tag{2}$$

The torque required to deflect the torsional spring through an angle of Θ is:

$$T = K\Theta \tag{3}$$

From the beam theory:

$$\theta_o = \frac{Ml}{(EI)_l} \tag{4}$$

Rearranging, it gives:

$$M = \frac{(EI)_l}{l}\theta_0 \tag{5}$$

Knowing that $T = M$ and $\Theta = \theta_o$, then the spring constant can be calculated as:

$$K = \frac{(EI)_l}{l} \tag{6}$$

The force F can be calculated as:

$$F = P\sqrt{n^2 + 1} \tag{7}$$

The angle ϕ can be expressed as:

$$\phi = arctg\left(\frac{1}{-n}\right) \tag{8}$$

The force that contributes to the deflection, F_t, is given by:

$$F_t = Fsen(\phi - \theta) \tag{9}$$

And the torque due to the force F_t is:

$$T = F_t\left(L + \frac{l}{2}\right) \tag{11}$$

The maximum stress is:

$$\sigma_{max} = \frac{Fac}{I}, \tag{12}$$

where c is the distance to the neutral axis in the small-length flexural pivot.

3. RESULTS AND DISCUSSIONS

3.1 Choosing the electric current value

Emiliavaca (2016) showed that the NiTi micro spring is already at the austenitic phase at room temperature. For different strains on the spring, inducing detwinned martensitic phase, the new austenitic transformation occurs before the temperature reaches 40 °C and the spring keeps the heat at a maximum of 50 °C.

Here, the temperature vs. time test was carried out with different electric currents to determine which one can make the spring reach 50 °C more rapidly, which gives time to the spring shift to the austenitic phase, with the spring deformed at 400%. The temperature behavior obtained is shown in Figure 3.

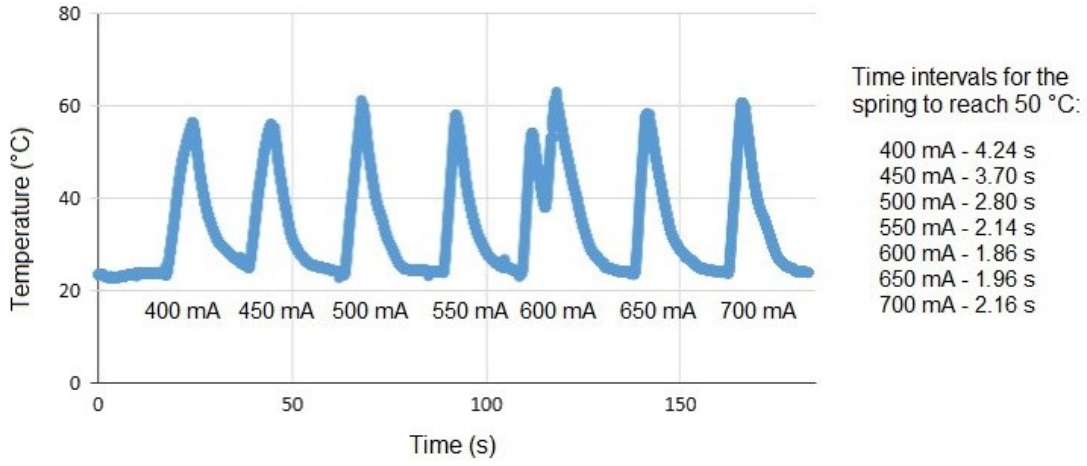

Figure 3. Temperature vs. Time curves for different electric currents and time intervals necessary for the spring to reach 50 °C.

It is possible to notice that, with the increase in the electric current value, the necessary time for the spring to reach 50 °C decreases, but after certain current values, the time increases as well. Another point to be considered is that the spring can burn if the electric current becomes too high. Thus, from analysis, a current of 550 mA, with an activation time of 2.2 s, was chosen.

3.2 Dimensioning the robot leg

Each leg of the robot was modeled using the pseudo-rigid-body model described by Howell (2001) and presented in section 2.3. The leg was considered as a beam connected to the body by a small flexible beam, which represents the small-length-flexural pivot.

Emiliavaca (2016) determined through a specific thermomechanical analysis that the spring previously deformed at 360% can produce a force of 4.5 N when contracted to 300% and 3.0 N when elongated to 400%.

These deformation values were used in the robot design, considering that the actuated spring will contract and pull the leg with a force of 4.5 N, while the opposite spring, which is connected to the other leg, will generate an opposite force of 3.0 N, since a bar connects the two legs. The distance between the forces is 15 mm. This model is illustrated in the simplified free body diagram shown in Figure 4.

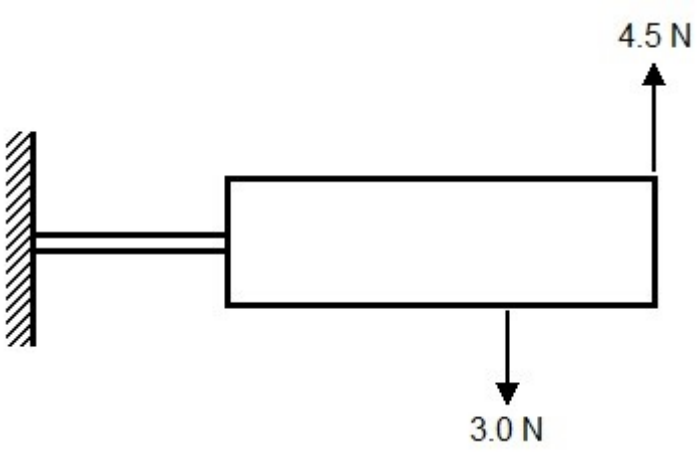

Figure 4. Top view of the simplified free body diagram of the robot leg.

With the model and forces established, the next step was to define the values for the main dimensions of the leg, as pointed out in Figure 5.

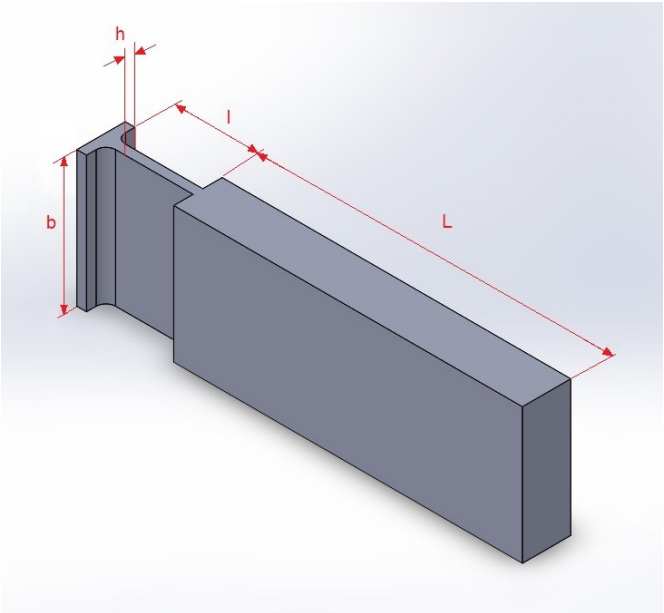

Figure 5. Main dimensions of the robot leg.

Using Equations (1) to (12), two graphs were generated for each dimension, containing the stress (σ_{max}) and deflection (dy), both as a function of the respective dimension. For each graph, the other parameters were kept constant to analyze the variation of stress and deflection with the change of one dimension only. These results are shown in Figures 6 to 9.

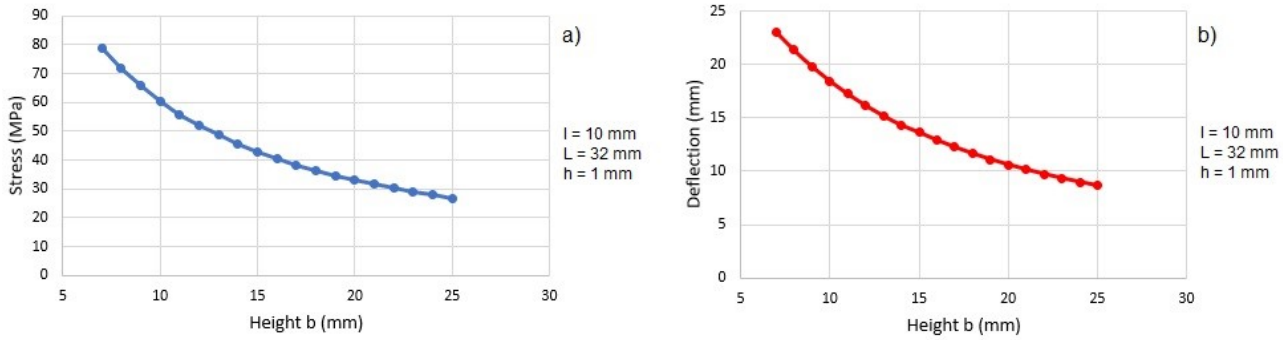

Figure 6. Stress as a function of height *b* (a) and deflection as a function of height *b* (b).

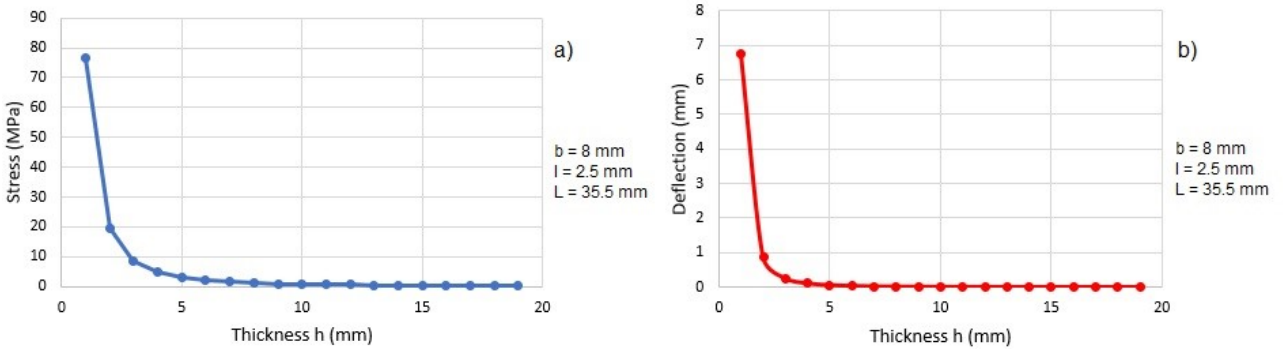

Figure 7. Stress as a function of thickness *h* (a) and deflection as a function of thickness *h* (b).

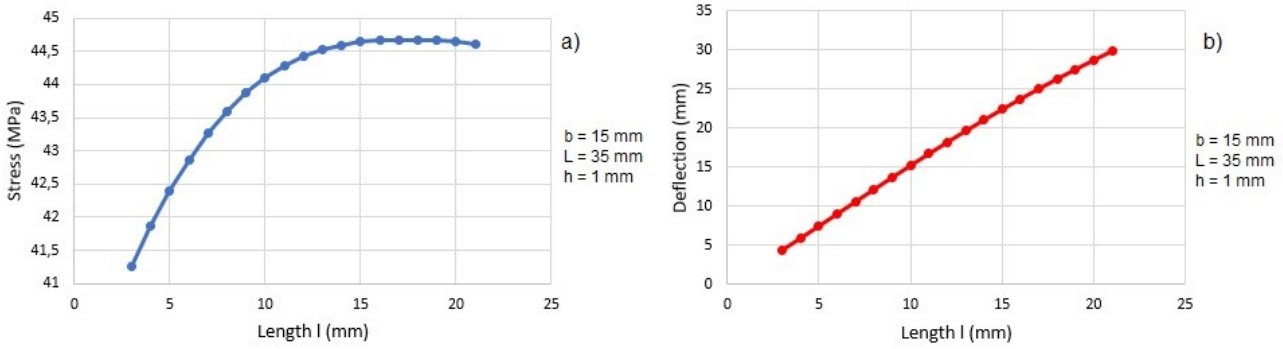

Figure 8. Stress as a function of length *l* (a) and deflection as a function of length *l* (b).

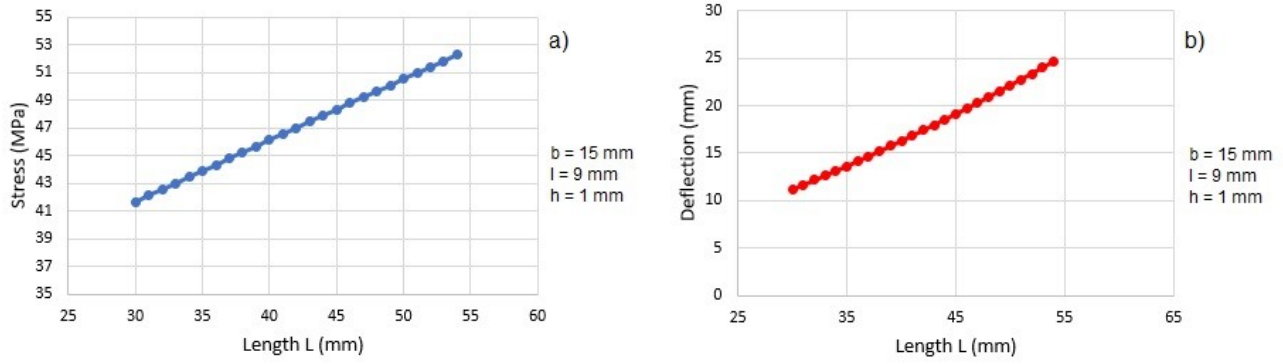

Figure 9. Stress as a function of length *L* (a) and deflection as a function of length *L* (b).

It is possible to observe that depending on how the parameters are changed, it is possible to reduce a large quantity of stress, but in counterpart the deflection, which is the displacement of the leg, is also reduced.

Thus, after analyzing the curves, the final values were determined as shown in Table 1.

Table 1. Final dimensions of the leg, deflection and stress.

Determined values	
Height *b*, mm	14.00
Thickness *h*, mm	1.00
Length *l*, mm	9.00
Length *L*, mm	36.00
Deflection, mm	14.94
Maximum stress, MPa	47.16

With the dimensions of Table 1, a mechanical simulation was realized by the finite element method (FEM) using ANSYS software with a CAD model of the leg to verify the accuracy of the calculated values of deflection and stress. The results are shown in Figures 10 and 11.

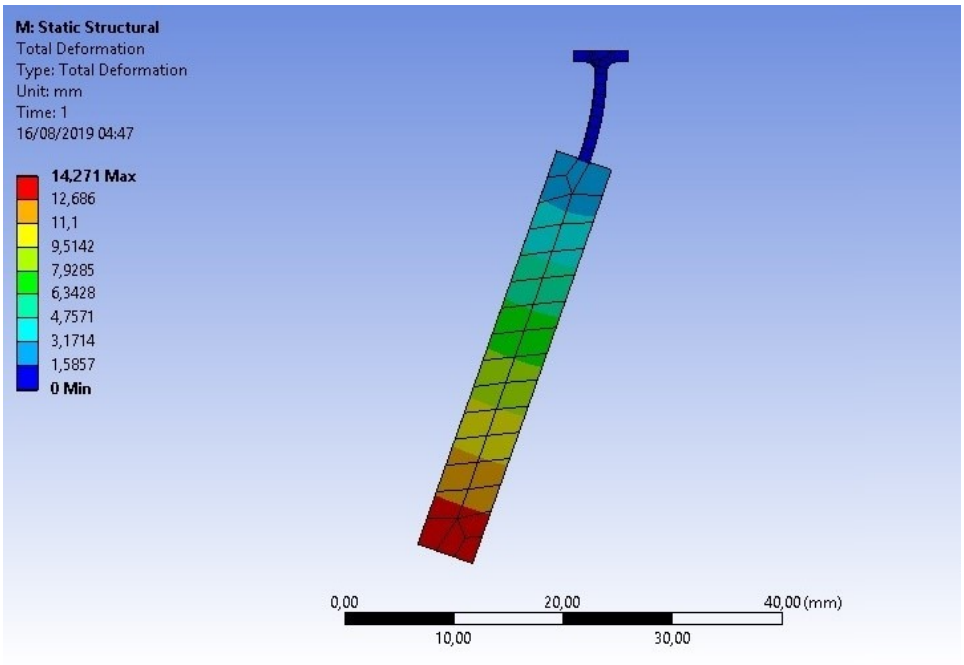

Figure 10. Simulated deflection of the leg.

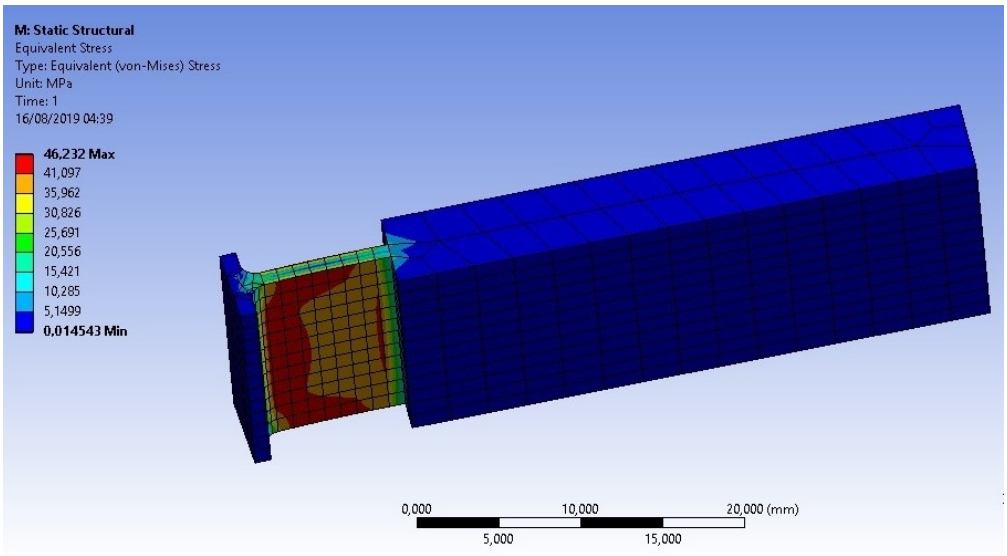

Figure 11. Simulated stress on the leg.

It is possible to verify that the simulated values for deflection and stress are in agreement to the ones calculated and shown in Table 1.

3.3 Prototype test

After dimensioning and simulating the mechanism, the robot was designed in a CAD software and then built by 3D printing, using the MakerBot 3D printer. The results are shown in Figure 12.

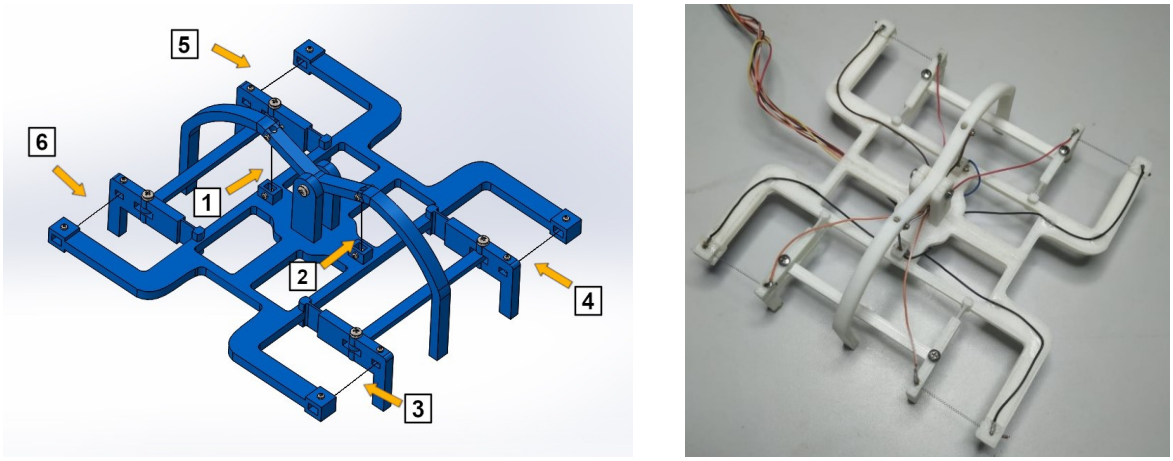

Figure 12. CAD model of the robot (a) and prototype manufactured by 3D printing (b). The numbers indicate the NiTi SMA micro spring actuators.

The performance of this novel compliant SMArt Robot was analyzed by measuring the robot velocity using the test bench shown in Figure 13 and the same spring activation sequence used in Hora (2016). For the preliminary tests two electric currents were used: 400 mA, with an activation time of 6 s, which was the best result obtained from Hora (2016), and 550 mA with an activation time of 2.2 s, to compare both results and verify which one would be better.

For each current, a video was recorded and the average velocity was estimated. For 400 mA the average velocity was 10.9 mm/min, while the average velocity for 550 mA was 21.5 mm/min.

In the literature, Chang-Ju et al. (2004), also using SMA micro spring actuators in a wheeled robot, obtained an average final speed of 50 mm/min. On the other hand, Kim et al. (2006) obtained an average final velocity of 10 mm/min with an earthworm robot also driven by SMA micro springs.

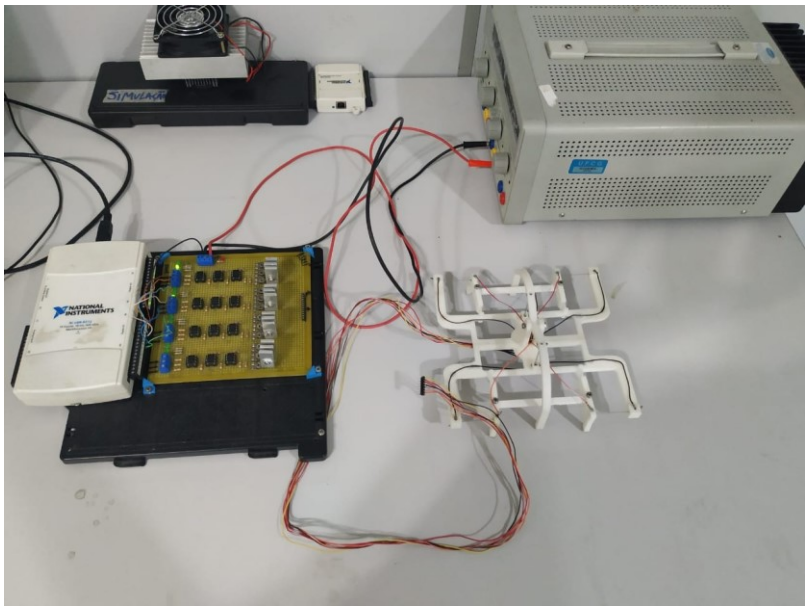

Figure 13. Robot over the test bench, with the control system and power supply.

Despite the fact that both results were inferior to the velocities obtained by Hora (2016), it is clear that the electric current chosen has significant impact on the robot performance, since it determines how quickly the SMA spring shifts to another phase.

4. CONCLUSIONS

In this work, it was possible to design and build a 3D printed robot prototype using a methodology based on compliant mechanisms and actuated by SMA micro springs. The pseudo-rigid-body approach, used to model and design the robot legs, was accurate and in agreement with the FEM simulations.

The effect of the electric current was also observed, since the current chosen had a significant improvement on performance compared to a lower current. For 400 mA the average velocity was 10.9 mm/min, while the velocity for 550 mA was 21.5 mm/min. These values are compatible with those of other low-speed SMA robot prototypes found in the literature. Therefore, the overall performance still needs improvements, which could be a controlled cooling system to the springs or a more sophisticated compliant mechanism.

5. ACKNOWLEDGEMENTS

The authors thank the Lab of Active Materials and Structures (LaMMEA) from UFCG for providing all the materials and structure needed to accomplish this work, as well as its team for all the support provided. The authors also thank CAPES for the financial support given to the Mechanical Engineering PET group from UFCG.

6. REFERENCES

Chang-Ju, W., Pei-Sun, M., and Qin, Y., 2004. “A prototype micro-wheeled-robot using SMA actuator”. Sensors and Actuators A: Physical, Vol. 113, pp. 94-99.

Doroftei, I. and Stirbu, B., 2014. “Application of Ni-Ti shape memory alloy actuators in a walking micro-robot”. *Mechanika*, Vol. 20, No. 1, pp. 70-79.

Emiliavaca, A., 2016. “SMArt morphing wing: an adaptive wing prototype actuated by shape memory alloy micro springs (in Portuguese)”. Master’s Thesis, Graduate Program in Mechanical Engineering, Federal University of Campina Grande, Campina Grande, Brazil.

Hora, R.A. 2016., “SMArt Robot – A hexapod robot prototype made by 3D printing and actuated by shape memory alloy micro springs (in Portuguese)”. Bachelor’s Thesis, Undergraduate Program in Mechanical Engineering, Federal University of Campina Grande, Campina Grande, Brazil.

Howell, L.L., 2001. *Compliant Mechanisms*. John Wiley & Sons, New York.

Kim, B., Lee, M.G., Lee, Y.P., Kim, Y., and Lee, G., 2006. “An earthworm-like micro robot using shape memory alloy actuator”. Sensors and Actuators A: Physical, Vol. 125, pp. 429-437.

Lan, C.-C. and Yang, Y.-N., 2009. “A computational design method for a shape memory alloy wire actuated compliant finger”. *Journal of Mechanical Design*, Vol. 131, p. 021009.

Motzki, P., 2020. “Efficient SMA actuation – design and control concepts”. In *Proceedings of The 1st International Electronic Conference on Actuator Technology: Materials, Devices and Applications.*

Reynaerts, D. and Van Brussel, H., 1991. “A SMA high performance actuator for robot hands”. Journal de Physique IV.

Song, M.-G., Baek, H.-W., Park, N.-C., Park, K.-S., Yoon, T., Park, Y.-P., and Lim, S.-C., 2010. “Development of small sized actuator with compliant mechanism for optical image stabilization”. *IEEE Transactions on Magnetics*, Vol. 46, No. 6, pp. 2369-2372.

Srinivasan, A.V. and McFarland, M.D., 2001. *Smart Structures Analysis and Design*. Cambridge University Press.

7. RESPONSIBILITY NOTICE

The authors are the only responsible for the printed material included in this paper.